

---

*This copy is for your personal, non-commercial use only.*

---

**If you wish to distribute this article to others**, you can order high-quality copies for your colleagues, clients, or customers by [clicking here](#).

**Permission to republish or repurpose articles or portions of articles** can be obtained by following the guidelines [here](#).

**The following resources related to this article are available online at [www.sciencemag.org](http://www.sciencemag.org) (this information is current as of July 23, 2011):**

**Updated information and services**, including high-resolution figures, can be found in the online version of this article at:

<http://www.sciencemag.org/content/333/6041/430.full.html>

**Supporting Online Material** can be found at:

<http://www.sciencemag.org/content/suppl/2011/07/20/333.6041.430.DC1.html>

<http://www.sciencemag.org/content/suppl/2011/07/21/333.6041.430.DC2.html>

This article **cites 32 articles**, 10 of which can be accessed free:

<http://www.sciencemag.org/content/333/6041/430.full.html#ref-list-1>

This article appears in the following **subject collections**:

Atmospheric Science

<http://www.sciencemag.org/cgi/collection/atmos>

$\vec{\epsilon}\delta O_n(\vec{r})$  by  $\frac{2e}{h}\vec{A}(\vec{r})$  where  $\vec{A}(\vec{r})$  is the electromagnetic vector potential, Eq. 5 becomes the GL free energy of a superconductor; its minimization in the long-distance limit yields  $\vec{A}(\vec{r}) = \frac{h}{2e}\vec{\nabla}\varphi(\vec{r})$  and thus quantization of its associated magnetic flux (22, 23). Analogously, minimization of Eq. 5 implies  $\delta O_n(\vec{r}) = \vec{l} \cdot \vec{\nabla}\varphi$  surrounding each topological defect (SOM e). Here, the vector  $\vec{l}$  is proportional to  $(\alpha_x, \alpha_y)$  and lies along the line where  $\delta O_n(\vec{r}) = 0$ . The resulting key prediction is that  $\delta O_n(\vec{r})$  will vanish along the line in the direction of  $\vec{l}$  that passes through the core of the topological defect, with  $O_n(\vec{r})$  becoming greater on one side and less on the other (Fig. 4B). Additional coupling to the smectic amplitude can shift the location of the topological defect away from the line of  $\delta O_n(\vec{r}) = 0$  (SOM e).

To test whether this GL model correctly captures the observed (Fig. 4, A and B)  $\delta O_n - \psi_s$  coupling in  $\text{Bi}_2\text{Sr}_2\text{CaCu}_2\text{O}_{8+\delta}$ , we extend Eq. 5 to include both  $\vec{S}_x$  and  $\vec{S}_y$  smectic modulations. We then simulate the profile of  $\delta O_n(\vec{r})$ , treating the phase and amplitude of smectic fields  $\psi_1(\vec{r})$  and  $\psi_2(\vec{r})$  (Fig. 2) as mean-field input that will determine  $\delta O_n(\vec{r})$  according to Eq. 5 (SOM e). Figure 4, C and D, shows the overlay of topological defect locations within the small boxes in Fig. 4A on  $\delta O_n(\vec{r})$  as simulated by using Eq. 5 (SOM e). This demonstrates directly how the GL functional associates fluctuations in  $\delta O_n(\vec{r})$  with the smectic topological defect locations in the fashion of Fig. 4B. The close similarity between the measured  $\delta O_n(\vec{r})$  in Fig. 4, E and F, and the simulation in Fig. 4, C and D, with cross-correlation coefficients of 56% and 62% demonstrates how the minimal GL functional of Eq. 5 captures the interplay between the measured  $\delta O_n(\vec{r})$  fluctuations (Fig. 4A) and disordered smectic modulations (Fig. 2). And, as expected with extrinsic disorder (36), the GL parameters vary somewhat from location to location (SOM f). Indeed, a simultaneous “gapmap” (SOM g) shows vividly how much additional (probably dopant-atom-related) disorder coexists with the phenomena analyzed here.

Our results can lead to advances in understanding of coexisting and competing electronic phenomena in underdoped cuprates (9–20). By identifying  $2\pi$  topological defects within the phase-fluctuating smectic states and that they are associated with the spatial fluctuations of the robust intra-unit-cell nematicity (18, 20), we demonstrated empirically a coupling between these two locally broken electronic symmetries of the cuprate pseudogap states. This allowed identification of a GL functional that explains how these phenomena coexist and predicts their interplay at the atomic scale. For example, the GL model explains why it is possible for the intra-unit-cell nematicity to have finite average  $\langle O_n(\vec{r}) \rangle \neq 0$  (Fig. 1C) even though the smectic modulations are disordered (Figs. 2 and 3) (18). This is because  $2\pi$  topological defects induce fluctuations of  $\delta O_n(\vec{r})$  with respect to  $\langle O_n(\vec{r}) \rangle$ , but the dislocation cores sit close to locations where  $O_n(\vec{r}) = \langle O_n(\vec{r}) \rangle$  and thus do not

disrupt this state directly (SOM e). Perhaps most importantly, if the tendency for intra-unit-cell nematicity to coexist with a disordered electronic smectic demonstrated here is ubiquitous to underdoped cuprates, which broken symmetry manifests at the macroscopic scale (9–20) depends on the coefficients in the GL functional and on other material-specific aspects, such as crystal symmetry. Therefore, the GL model introduced here provides a good starting point to address these issues and, eventually, the interplay between the different broken electronic symmetries and the superconductivity.

#### References and Notes

1. J. Zaanen, O. Gunnarsson, *Phys. Rev. B* **40**, 7391 (1989).
2. S. A. Kivelson, E. Fradkin, V. J. Emery, *Nature* **393**, 550 (1998).
3. S. A. Kivelson et al., *Rev. Mod. Phys.* **75**, 1201 (2003).
4. S. Sachdev, *Rev. Mod. Phys.* **75**, 913 (2003).
5. M. Vojta, *Adv. Phys.* **58**, 699 (2009).
6. V. J. Emery, S. A. Kivelson, J. M. Tranquada, *Proc. Natl. Acad. Sci. U.S.A.* **96**, 8814 (1999).
7. E.-A. Kim et al., *Phys. Rev. B* **77**, 184514 (2008).
8. E. Fradkin, S. A. Kivelson, M. J. Lawler, J. P. Eisenstein, A. P. Mackenzie, *Annu. Rev. Condens. Matter Phys.* **1**, 153 (2010).
9. J. M. Tranquada, B. J. Sternlieb, J. D. Axe, Y. Nakamura, S. Uchida, *Nature* **375**, 561 (1995).
10. J. M. Tranquada et al., *Nature* **429**, 534 (2004).
11. P. Abbamonte et al., *Nat. Phys.* **1**, 155 (2005).
12. Y.-J. Kim, G. D. Gu, T. Gog, D. Casa, *Phys. Rev. B* **77**, 064520 (2008).
13. X. F. Sun, K. Segawa, Y. Ando, *Phys. Rev. Lett.* **93**, 107001 (2004).
14. A. Kaminski et al., *Nature* **416**, 610 (2002).
15. B. Fauqué et al., *Phys. Rev. Lett.* **96**, 197001 (2006).
16. V. Hinkov et al., *Science* **319**, 597 (2008); 10.1126/science.1152309.
17. R. Daou et al., *Nature* **463**, 519 (2010).
18. M. J. Lawler et al., *Nature* **466**, 347 (2010).
19. Y. Li et al., *Nature* **455**, 372 (2008).
20. Y. Kohsaka et al., *Science* **315**, 1380 (2007); 10.1126/science.1138584.
21. N. D. Mermin, *Rev. Mod. Phys.* **51**, 591 (1979).

22. P. M. Chaikin, T. C. Lubensky, *Principles of Condensed Matter Physics* (Cambridge Univ. Press, Cambridge, 1995).
23. D. R. Tilley, J. Tilley, *Superfluidity and Superconductivity* (IOP Publishing, Bristol, UK, 1990).
24. P. G. de Gennes, *Solid State Commun.* **10**, 753 (1972).
25. J. Toner, D. R. Nelson, *Phys. Rev. B* **23**, 316 (1981).
26. Y. Kohsaka et al., *Nature* **454**, 1072 (2008).
27. J. Lee et al., *Science* **325**, 1099 (2009).
28. K. McElroy et al., *Phys. Rev. Lett.* **94**, 197005 (2005).
29. C. Howald, H. Eisaki, N. Kaneko, M. Greven, A. Kapitulnik, *Phys. Rev. B* **67**, 014533 (2003).
30. A. Del Maestro, B. Rosenow, S. Sachdev, *Phys. Rev. B* **74**, 024520 (2006).
31. J. A. Robertson, S. A. Kivelson, E. Fradkin, A. C. Fang, A. Kapitulnik, *Phys. Rev. B* **74**, 134507 (2006).
32. V. Cvetkovic, J. Zaanen, *Phys. Rev. Lett.* **97**, 045701 (2006).
33. M. Vojta, T. Vojta, R. K. Kaul, *Phys. Rev. Lett.* **97**, 097001 (2006).
34. G. Grüner, *Density Waves in Solids* (Addison-Wesley, Boston, 1994).
35. T. Choi et al., *Nat. Mater.* **9**, 253 (2010).
36. W. L. McMillan, *Phys. Rev. B* **12**, 1187 (1975).

**Acknowledgments:** We thank E. Fradkin, S. Kivelson, M. Norman, J. P. Sethna, and J. Tranquada for helpful discussions and communications. Theoretical studies at Cornell were supported by NSF grant DMR-0520404 to the Cornell Center for Materials Research and by NSF grant DMR-0955822. Experimental studies are supported by the Center for Emergent Superconductivity, an Energy Frontier Research Center headquartered at Brookhaven National Laboratory and funded by the U.S. Department of Energy under DE-2009-BNL-PMO15, as well as by a Grant-in-Aid for Scientific Research from the Ministry of Science and Education (Japan) and the Global Centers of Excellence Program for Japan Society for the Promotion of Science. The work at Harvard University was supported by DMR-0757145. The work at Leiden University was supported by the Nederlandse Organisatie voor Wetenschappelijk Onderzoek through a Spinoza Award. A.M. is grateful for the hospitality of E.-A.K.

#### Supporting Online Material

www.sciencemag.org/cgi/content/full/333/6041/426/DC1  
SOM Text

Figs. S1 to S3

Table S1

References

30 November 2010; accepted 2 June 2011

10.1126/science.1201082

## Atmospheric Carbon Injection Linked to End-Triassic Mass Extinction

Micha Ruhl,<sup>1,2\*</sup> Nina R. Bonis,<sup>1,3</sup> Gert-Jan Reichart,<sup>4</sup>  
Jaap S. Sinninghe Damsté,<sup>4,5</sup> Wolfram M. Kürschner<sup>1,6</sup>

The end-Triassic mass extinction (~201.4 million years ago), marked by terrestrial ecosystem turnover and up to ~50% loss in marine biodiversity, has been attributed to intensified volcanic activity during the break-up of Pangaea. Here, we present compound-specific carbon-isotope data of long-chain *n*-alkanes derived from waxes of land plants, showing a ~8.5 per mil negative excursion, coincident with the extinction interval. These data indicate strong carbon-13 depletion of the end-Triassic atmosphere, within only 10,000 to 20,000 years. The magnitude and rate of this carbon-cycle disruption can be explained by the injection of at least  $\sim 12 \times 10^3$  gigatons of isotopically depleted carbon as methane into the atmosphere. Concurrent vegetation changes reflect strong warming and an enhanced hydrological cycle. Hence, end-Triassic events are robustly linked to methane-derived massive carbon release and associated climate change.

The end-Triassic mass extinction (ETME) [~201.4 million years ago (1)], one of the five major extinction events of the Phan-

erozoic (2), is marked by up to 50% marine biodiversity loss and major terrestrial ecosystem changes (2–5). This event closely matches a

distinct and globally observed negative carbon-isotope excursion (CIE) in  $\delta^{13}\text{C}_{\text{TOC}}$  records (TOC: total organic carbon) (6, 7) and a potential fourfold increase in atmospheric  $\text{CO}_2$  concentrations (8). Previously, the end-Triassic C-cycle perturbation has been attributed to large-scale carbon release caused by a major volcanic episode, with emplacement of the Central Atlantic Magmatic Province (CAMP) during the break-up of Pangaea. However, deposition of this large igneous province continued for at least  $\sim 600$  ky (ky, thousand years) (9, 10), much longer than the  $\sim 20$ - to 40-ky duration of the end-Triassic extinction event (11, 12). The magnitude of the observed negative CIE also varies largely between different geological basins, possibly due to changes in source and preservation of the sedimentary organic matter. These observations question the reality of an end-Triassic global carbon cycle turnover and its potential causal relationship to the extinction event. We determined compound-specific C-isotope records from the western Tethys Ocean [including the global stratotype section and point (GSSP) for the base of the Jurassic], which span the ETME. Changes in the stable carbon isotopic composition of long-chain *n*-alkanes, derived from epicuticular plant waxes, directly reflect changes in the carbon isotopic composition of  $\text{CO}_2$  in the atmosphere. Furthermore, the  $\delta^{13}\text{C}$  of these organic molecules is, depending on burial history, unaffected by diagenetic alteration of organic matter (13). Hence, this allows accurate reconstruction of the end-Triassic C-cycle perturbation in a biostratigraphically well-constrained framework.

Sediments for this study are from an upper Rhaetian (latest Triassic) interval of 54 cm in the Kuhjoch and 52 cm in the Hochalplgraben outcrops (7). These sediments were deposited in the intraplateform Eiberg Basin at the continental margin of the western Tethys Ocean (14). The studied interval in both sections directly succeeds the transition from limestones of the Kössen Formation (Fm) to marls of the Kendlbach Fm and coincides with marine and terrestrial extinctions and assemblage changes (Fig. 1). Long-chain *n*-alkanes ( $\text{C}_{23}$  to  $\text{C}_{35}$ ) are preserved in these  $>200$ -million-year-old, but thermally immature (15), sediments and originate from higher-plant leaf waxes, with moderate odd-over-even carbon

number predominance (16). The weighted-average of the stable carbon isotopic composition of the odd-numbered  $\text{C}_{23}$  to  $\text{C}_{35}$  *n*-alkanes shows a  $\sim 8.5$  per mil (‰) negative excursion from Rhaetian base values of  $\sim -29$ ‰ (Fig. 2). The observed negative excursion in compound-specific C-isotope data strongly suggests  $^{13}\text{C}$  depletion of the terrestrial higher-plant carbon reservoir, and hence is sound evidence for end-Triassic atmospheric- $^{13}\text{C}$  depletion coinciding with the ETME. This negative CIE in our molecular records is  $>2.5$ ‰ stronger than in  $\delta^{13}\text{C}_{\text{TOC}}$  records from Austria and the UK (6, 7) and 5.5‰ stronger than previously assumed for the modeled end-Triassic negative CIE (17). It is also two times as large as observed in the Newark-Hartford basin compound-specific  $\delta^{13}\text{C}$  record (10).

Major vegetation changes could have modified the magnitude of the end-Triassic negative CIE in compound-specific C-isotope records because of differential carbon isotopic fractionation among plant groups. Palynological data show a strong increase of Cheirolepidiacean (*Classopollis meyeriana*) conifer pollen concurrent with the onset of the observed negative CIE (18). A rapid transition from a mixed angiosperm-conifer flora to a purely angiosperm flora at the Paleocene-Eocene Thermal Maximum (PETM), however, amplified the observed negative CIE by 1 to 2‰ (19). Also, modern conifer-derived *n*-alkanes are relatively enriched in  $^{13}\text{C}$  because of a lower stomatal conductance relative to other plant groups (20). Assuming that physiological mechanisms in Mesozoic conifers were similar to those in conifers of the Cenozoic and today, the observed 8.5‰ end-Triassic higher-plant *n*-alkane  $\delta^{13}\text{C}$  excursion may thus even be dampened relative to atmospheric values. The smaller magnitude of this excursion in the Newark-Hartford  $\delta^{13}\text{C}_{n\text{-alkane}}$  record may be due to a lower sampling resolution during the ETME (10).  $\delta^{13}\text{C}_{n\text{-alkane}}$  values in this record may also be affected by thermal degradation of *n*-alkanes or mixing of organic sources, as suggested by *n*-alkane chain-length distribution and large variations between  $\delta^{13}\text{C}_{n\text{-alkane}}$ ,  $\delta^{13}\text{C}_{\text{TOC}}$ , and  $\delta^{13}\text{C}_{\text{wood}}$  (10). Nevertheless, the similar trend in compound-specific C-isotope records during the ETME in North America (10) and the Western Tethys Ocean (this study) strongly suggests major end-Triassic atmospheric  $^{13}\text{C}$  depletion.

The end-Triassic negative CIE in  $\delta^{13}\text{C}_{\text{TOC}}$  records was, based on model calculations, previously ascribed to the release of  $\sim 8000$  to 9000 gigatons (Gt) of carbon as volcanogenic gaseous  $\text{CO}_2$  from the CAMP with subsequent destabilization of  $\sim 5000$  Gt of carbon from the methane-hydrate reservoir (17). Also, recent  $P_{\text{CO}_2}$  (partial pressure of  $\text{CO}_2$ ) estimates from pedogenic carbonates, succeeding subsequent CAMP basalt units in eastern North American rift basins, suggest major basaltic  $\text{CO}_2$  outgassing (21). However, this modeled release of carbon from two reservoirs results in a  $\sim 3$ ‰ depletion of the exogenic carbon pool only. The onset of the observed negative CIE

probably occurred within  $\sim 10$  to 20 ky, based on the astronomically constrained  $\sim 20$ - to 40-ky duration of the complete event (10–12). This implies a rapid release of large amounts of isotopically depleted carbon to the end-Triassic atmosphere, coincident with the ETME. The  $\sim 8.5$ ‰ magnitude and the short ( $\sim 20$  to 40 ky) duration of the observed negative CIE do not, therefore, match with CAMP-related  $\text{CO}_2$  release as the main source for isotopically depleted carbon. A simple mass balance calculation using end-Triassic boundary conditions (16, 17) shows that  $\sim 8.5$ ‰ atmospheric- $^{13}\text{C}$  depletion can also be explained by the release of  $\sim 12,000$  Gt of carbon as methane from clathrates (with  $\delta^{13}\text{C}$  values of  $-60$ ‰). Alternatively, thermal metamorphism of subsurface organic-rich strata, associated with sill intrusions and flood basalt emplacement, was proposed as a major source of  $^{13}\text{C}$ -depleted thermogenic methane to the end-Permian, Rhaetian, Toarcian, and Eocene atmosphere (22–25). It possibly also contributed to the magnitude of the end-Triassic C-cycle perturbation at the ETME (23, 26). Carbon release purely from this source (with  $\delta^{13}\text{C}$  values of  $-35$  to  $-50$ ‰) would involve an input of possibly as much as 38,000 Gt. None of these mechanisms is mutually exclusive, and all three may have contributed to the release of  $^{13}\text{C}$ -depleted carbon at the ETME, with thermogenic methane and gaseous  $\text{CO}_2$  release from CAMP initiating a positive feedback in the global exogenic carbon cycle, causing the release of methane from clathrates. The relative contribution of these end members for  $^{13}\text{C}$ -depleted carbon release is yet unknown. Continued carbon release from primary outgassing or contact metamorphism during CAMP emplacement (21) likely caused prolonged early Jurassic  $P_{\text{CO}_2}$  increase and decreased  $\delta^{13}\text{C}_{\text{TOC}}$  values (12). However, given the duration and magnitude of the observed end-Triassic negative CIE, a strong contribution from the methane-clathrate reservoir may be likely.

The injection of  $\sim 12,000$  to 38,000 Gt of carbon during the ETME probably had a profound impact on global climate. Statistical analyses of palynological data spanning this time interval (16) show a strong warming event and an enhanced hydrological cycle directly coinciding with the onset of the negative CIE (Fig. 2). Marine and terrestrial assemblage changes and extinctions directly coincide with the onset of this warming event (Fig. 2). This suggests a strong causal relationship between massive carbon release, associated climate change, and terrestrial and marine ecosystem turnover. Terrestrial ecosystem changes have likely been further enhanced by the release of toxic gases (e.g., sulfur dioxide) (26). Massive carbon release to the atmosphere and subsequently the ocean also has strong effects on ocean acidification (27). At the ETME, this resulted in decreased carbonate precipitation and possibly dissolution, leading to reduced marine ecosystem stability and extinctions (28).

<sup>1</sup>Palaeoecology, Institute of Environmental Biology, Faculty of Science, Utrecht University, Budapestlaan 4, NL-3584 CD, Utrecht, Netherlands. <sup>2</sup>Nordic Centre for Earth Evolution (NordCEE), Natural History Museum of Denmark, University of Copenhagen, Øster Voldgade 5-7, DK-1350, Copenhagen K, Denmark. <sup>3</sup>Shell Global Solutions International B.V., Kessler Park 1, 2288 GS, Rijswijk, Netherlands. <sup>4</sup>Molecular Biogeochemistry, Department of Earth Sciences, Faculty of Geosciences, Utrecht University, Post Office Box 80.021, NL-3508 TA, Utrecht, Netherlands. <sup>5</sup>Department of Marine Organic Biogeochemistry, NIOZ Royal Netherlands Institute for Sea Research, Post Office Box 59, 1790 AB, Den Burg, Netherlands. <sup>6</sup>Department of Geosciences, University of Oslo, Post Office Box 1047, Blindern, 0316 Oslo, Norway.

\*To whom correspondence should be addressed. E-mail: micharuhl@gmail.com

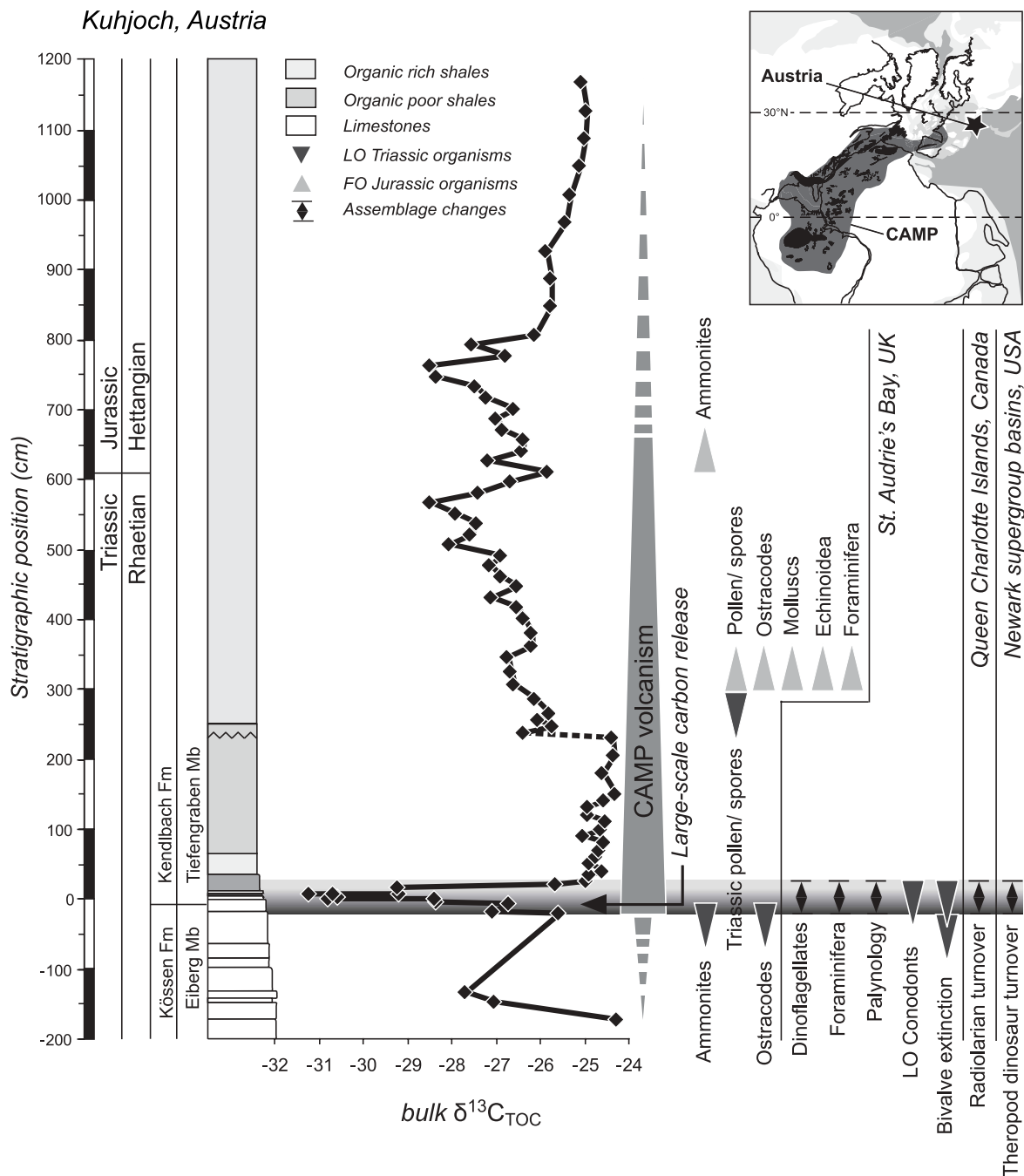


**Fig. 1.** End-Triassic mass extinction event coincides with  $\delta^{13}\text{C}_{\text{TOC}}$  negative excursion. The  $\delta^{13}\text{C}_{\text{TOC}}$  record from Kuhjoch (7), the GSSP for the base of the Jurassic (47°41'15"N, 13°21'30"E). The end-Triassic negative CIE closely

matches marine extinctions and continental and marine assemblage changes (3, 6, 14, 34) (LO, last occurrence; FO, first occurrence). The negative CIE stratigraphically coincides with the onset of CAMP emplacement (11).

Similar events of rapid carbon release to the atmosphere [e.g., at the PETM (29) and in the early Toarcian (30)] suggest a ~100-ky recovery period for the  $\delta^{13}\text{C}$  composition of exchangeable carbon reservoirs, in line with the residence time of carbon in the exogenic carbon pool (31). A relatively short duration of the observed negative CIE at the ETME may be attributed to enhanced surface-ocean productivity and increased burial of carbon at the continental margins (18). Diminished background release of isotopically light

carbon, due to changes in the gas-hydrate capacitor (31), may have further enhanced rapid recovery of the  $\delta^{13}\text{C}$  signal of the exogenic carbon pool. Furthermore, a sea-level lowstand at the ETME possibly enhanced erosion of the extensive Triassic carbonate ramps and dilution of the exchangeable carbon reservoirs with relatively enriched carbon.

The ETME interval, with rapid and large-scale carbon release, may be regarded as a natural deep-time analog to today's anthropogenic carbon emis-

sions. Cumulative anthropogenic carbon release of >5000 Gt (27) likely will enhance greenhouse warming by several degrees (32) and substantially lower oceanic pH values (27). Earth's biosphere also is projected to experience major disruption of ecosystems, with associated loss of biodiversity (33). A direct link between massive carbon release and the ETME suggests that modern-day ecosystems could experience a further loss in biodiversity, not only by habitat reduction but also by carbon release-driven rapid climate changes.

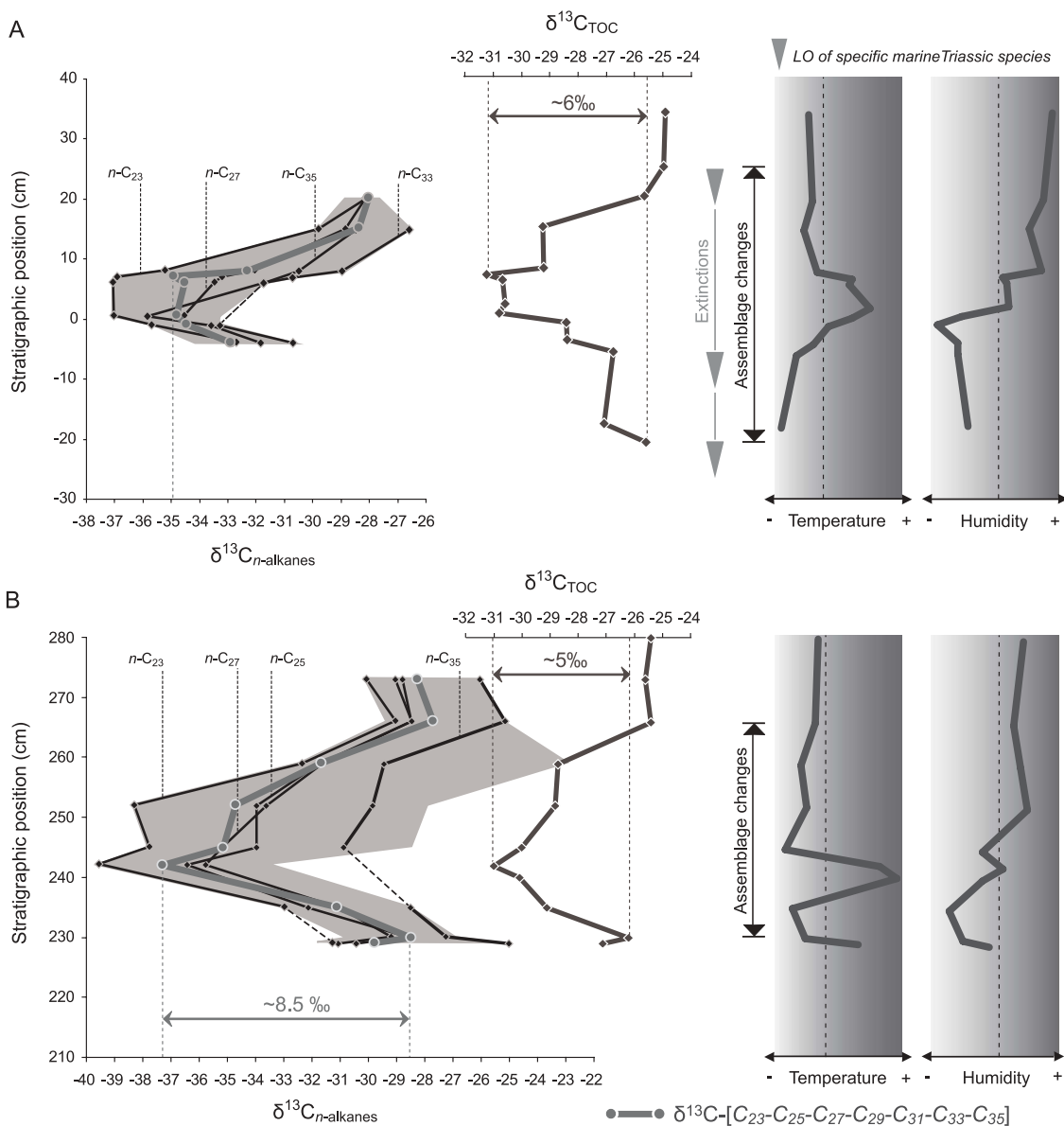


**Fig. 2.** *N*-alkane biomarker C-isotope and climate proxy records. The end-Triassic mass-extinction interval is marked by a distinct negative CIE in  $\delta^{13}\text{C}_{n\text{-alkane}}$  records from (A) Kuhjoch and (B) Hochalplgraben ( $47^{\circ}28'20''\text{N}$ ,  $11^{\circ}24'42''\text{E}$ ). The  $\sim 8.5\%$  magnitude of the negative CIE in the weighted-average  $\delta^{13}\text{C}_{(C_{23}\text{-}C_{25}\text{-}C_{27}\text{-}C_{29}\text{-}C_{31}\text{-}C_{33}\text{-}C_{35})}$  record of Hochalplgraben is  $\sim 3.5\%$  larger than observed in the  $\delta^{13}\text{C}_{\text{TOC}}$  record of the same section. The black curves show individual *n*-alkane C-isotope records for both sections. The

shaded areas show the bandwidth of  $\delta^{13}\text{C}_{C_{23}}$  to  $\delta^{13}\text{C}_{C_{35}}$  values per sample, in both sections. The extracted amount of *n*-alkanes from the lower three  $\delta^{13}\text{C}_{\text{TOC}}$  samples from Kuhjoch was too low for reliable  $\delta^{13}\text{C}_{n\text{-alkane}}$  measurements. The (onset of the) observed negative CIE coincides in both sections with increased continental temperatures and an enhanced hydrological cycle, based on statistical analyses of terrestrial palynomorph distributions (16).

#### References and Notes

- B. Schoene, J. Guex, A. Bartolini, U. Schaltegger, T. J. Blackburn, *Geology* **38**, 387 (2010).
- D. M. Raup, J. J. Sepkoski Jr., *Science* **215**, 1501 (1982).
- P. E. Olsen *et al.*, *Science* **296**, 1305 (2002).
- J. C. McElwain, P. J. Wagner, S. P. Hesselbo, *Science* **324**, 1554 (2009).
- J. J. Sepkoski, in *Global Events and Event Stratigraphy in the Phanerozoic*, O. H. Walliser, Ed. (Springer, Berlin, 1996) pp. 35–51.
- S. P. Hesselbo, S. A. Robinson, F. Surlyk, S. Piasecki, *Geology* **30**, 251 (2002).
- M. Ruhl, W. M. Kürschner, L. Krystyn, *Earth Planet. Sci. Lett.* **281**, 169 (2009).
- J. C. McElwain, D. J. Beerling, F. I. Woodward, *Science* **285**, 1386 (1999).
- A. Marzoli, P. R. Renne, E. M. Piccirillo, M. Ernesto, G. Bellieni, A. De Min, *Science* **284**, 616 (1999).
- J. H. Whiteside, P. E. Olsen, T. Eglinton, M. E. Brookfield, R. N. Sambrotto, *Proc. Natl. Acad. Sci. U.S.A.* **107**, 6721 (2010).
- M. H. L. Deenen *et al.*, *Earth Planet. Sci. Lett.* **291**, 113 (2010).
- M. Ruhl *et al.*, *Earth Planet. Sci. Lett.* **295**, 262 (2010).
- R. D. Pancost, C. S. Boot, *Mar. Chem.* **92**, 239 (2004).
- A. von Hillebrandt, L. Krystyn, W. M. Kürschner, *International Subcommittee on Jurassic Stratigraphy Newsletter* **34** 1, 2 (2007); <http://jurassic.earth.ox.ac.uk/newsletters>
- M. Ruhl, H. Veld, W. M. Kürschner, *Earth Planet. Sci. Lett.* **292**, 17 (2010).
- Supporting Online Material is available at *Science* Online.
- D. J. Beerling, R. A. Berner, *Global Biogeochem. Cycles* **16**, 1036 (2002).
- N. R. Bonis, M. Ruhl, W. M. Kürschner, *Palaeogeogr. Palaeoclimatol. Palaeoecol.* **290**, 151 (2010).
- S. Schouten *et al.*, *Earth Planet. Sci. Lett.* **258**, 581 (2007).
- N. Pedentchouk, W. Sumner, B. Tipple, M. Pagani, *Org. Geochem.* **39**, 1066 (2008).
- M. F. Schaller, J. D. Wright, D. V. Kent, *Science* **331**, 1404 (2011).
- H. Svensen *et al.*, *Earth Planet. Sci. Lett.* **277**, 490 (2009).
- M. Ruhl, W. M. Kürschner, *Geology* **39**, 431 (2011).
- H. Svensen *et al.*, *Earth Planet. Sci. Lett.* **256**, 554 (2007).
- H. Svensen *et al.*, *Nature* **429**, 542 (2004).
- B. van de Schootbrugge *et al.*, *Nat. Geosci.* **2**, 589 (2009).

